Resource Efficient and Robust RSMA for Visible Light Communications

Jianfei Hu, *Student Member, IEEE*, Chen Sun, *Member, IEEE*, Jiaheng Wang, *Senior Member IEEE*, Xiqi Gao, *Fellow, IEEE*, Liang Xia, and Qixing Wang

***Abstract*—Spectral efficiency (SE) and energy efficiency (EE) are two main metrics for the transmit design in Visible Light Communications (VLC). However, the SE-optimal and EE-optimal strategies may be in conflict with each other to some extent. In this paper, we investigate the the tradeoff between EE and SE in rate splitting multiple access (RSMA)-aided VLC systems to maximize the system resource efficiency (RE) taking both perfect and imperfect channel state information (CSI) into consideration. For the scenarios with perfect CSI, we explore the joint precoding design and common rate allocation to maximize the RE of RSMA-aided VLC systems under the constraints of quality of service (QoS) and linear operation region (LoR) of LED, and propose a primal-dual-gradient-based precoding strategy. Furthermore, in the presence of CSI estimation errors, we propose a worst-case robust precoding design by exploiting quadratic transform and $\mathcal{S}$-Procedure. Numerical results indicate that the proposed resource efficient RSMA algorithm achieves the tradeoff between EE and SE.**

***Index Terms*—Rate splitting multiple access, resource efficiency, energy efficiency, spectral efficiency, tradeoff.**

I. Introduction

WIRELESS data traffic is exponentially growing, with most of which is generated in indoor spaces such as homes and office buildings [1]. Moreover, the ongoing issues of the spectrum resource scarcity in conventional radio frequency (RF) communications necessitate the development of innovative wireless technologies. Visible light communications (VLC), with its inherent security features, resistance to electromagnetic interference, and access to abundant unlicensed spectrum, is viewed as a viable and effective complement to RF communications [2].

Despite these remarkable benefits of VLC, the limited modulation bandwidth and low optical power of commercial LEDs impede the realization of VLC system's full potential [3]. Therefore, both academic and industry scientists have made significant efforts to overcome the LED constraints, with the aim to improve spectral efficiency (SE) and energy efficiency (EE) of VLC systems. The design of effective multiple access schemes paves the way for achieving higher efficiency in VLC systems [4].

J. Hu, C. Sun, J. Wang and X. Gao are with the National Mobile Communications Research Laboratory, School of Information Science and Engineering, Southeast University, Nanjing 210096, China, and also with Purple Mountain Laboratories, Nanjing 211111, China (e-mail: jianfeihu@seu.edu.cn; sunchen@seu.edu.cn; jhwang@seu.edu.cn; xqgao@seu.edu.cn).

Liang Xia and Qixing Wang are with the China Mobile Research Institute, Beijing 100053, China (e-mail: xialiang@chinamobile.com; wangqixing@chinamobile.com).

To enhance the system SE and EE, the concept of rate splitting multiple access (RSMA) was introduced in RF communications [5]–[7]. RSMA operates by dividing the message of each user into public and private components. Subsequently, all the public components are encoded together into a unified stream for decoding by all receivers, while the private components are exclusively decoded by their respective users. Research has demonstrated that RSMA is capable of reducing the complexity of both BS and users while outperforming space division multiple access (SDMA) and non-orthogonal multiple access (NOMA) regardless of channel state information (CSI) accuracy and network load [7], [8].

To harness the advantages of RSMA in RF communications, researchers have devoted extensive efforts in resource allocation, transmission design and application extension. In general, there are three lines of research for RSMA, namely SE optimization, EE optimization and EE-SE tradeoff. In the literature, much attention has been dedicated to dealing with SE optimization problem. For example, a linear precoding strategy is proposed in [9] to maximize the system SE in downlink MIMO, where the LogSumExp technique is adopted to convert the primal problem into a tractable problem of maximizing the sum of generalized Rayleigh quotients. The authors in [10] consider the sum-rate maximization problem and propose a fractional programming (FP) and fixed point iteration based algorithm. Although SE metric plays a crucial part in system design, we have to notice that the EE metric has attracted much attention due to the energy dilemmas and global warming concerns. The paper [11] investigates the EE of RSMA-aided downlink MISO systems and proposes an SCA-based beamforming design to address the EE maximization problem. The joint precoding and reconfigurable intelligent surfaces (RIS) control problem is considered in [12] to optimize the system EE, and a two-stage scheme based on SCA is proposed to tackle this non-convex fractional problem. Compared to the aforementioned works that concentrate on a single optimization criteria, fewer researchers investigate the EE-SE balance. In [13], the authors transform the joint EE and SE multi-objective optimization into a single-objective problem by weighted-power and weighted-sum approaches, and propose an SCA-based iterative algorithm to achieve the EE-SE tradeoff. Authors in [14] investigate an integration of RSMA and active RIS to strike a desired EE-SE tradeoff, and a two-stage alternating optimization scheme is proposed to tackle the tradeoff issue. It is worth noting that the mentioned studies are architected for RF communications, however, can not be directly transposed to VLC networks because of the

characteristics of intensity modulation and direct detection (IM/DD).

Moreover, research on RSMA for VLC networks is currently in early stages. For VLC systems, a closed-form expression of achievable rate lower bound for RSMA-based VLC systems is derived in [15] and the authors propose an iterative precoding design based on CCCP technique to enhance the spectral efficiency under both the electrical power and optical power constraints. Building upon the lower bound in [15], [16] and [17] investigate the spectral efficiency maximization problem and propose two different coordinated transmission strategies for multi-cell VLC systems. A linear precoding design is developed in [18] to enhance spectral efficiency and the performance between RSMA scheme and NOMA scheme is compared in multi-cell VLC networks. The authors in [19] consider the optimization problem of energy efficiency in both single and multi-cell scenarios, and propose an SCA-based precoding strategy for single-cell scenarios and a zero-forcing (ZF)-based precoding design for multi-cell scenarios, respectively.

A comprehensive review highlights RSMA's superior performance over SDMA and NOMA in various application scenarios. However, research on implementing RSMA in VLC is still in very early stages. Additionally, the aforementioned works only focus on a single criterion. The dynamic resource supply and demand differences among users result in that users' preference for SE and EE performance differs from each other. Unfortunately, the EE-optimal strategies and SE-optimal ones may conflict to some extent [20]. Thus, it is worthwhile to investigate how to strike an EE-SE balance in precoding design for achieving a more practical system performance.

Furthermore, note that successive interference cancellation (SIC) technique is employed in RSMA. The accuracy of CSI significantly influences the system performance, especially for SIC-dependent systems. In practice, the CSI estimation errors may result in residual interference and potential error propagation during SIC processing. Hence, designing robust RSMA holds significant importance for practical VLC networks. However, all the previous studies [16]–[19] for RSMA-aided VLC systems do not consider CSI estimation errors.

In view of the above problems, we investigate the tradeoff problem between EE and SE for RSMA-aided MISO VLC downlink systems with error bounded CSI. We adopt a flexible metric, termed as resource efficiency (RE) [20] [21], and explore the RE optimization to achieve a desired EE-SE balance. In conclusion, the principal contributions of this work can be outlined as follows.

- We explore the RE maximization problem to achieve an EE-SE balance under the quality of service (QoS) constraints and LED linear operation region constraints. To the best of our knowledge, this paper is the first to jointly optimize the system EE and SE and investigate the integration of RSMA into VLC systems. Note that RSMA provides a novel framework for multi-antenna networks, encompassing NOMA and SDMA as extreme schemes [8]. As a result, investigating the EE-SE tradeoff problem for RSMA-assisted VLC systems simultaneously addresses the EE-SE tradeoff issues for NOMA and SDMA-based systems.
- In scenarios with perfect CSI, we jointly optimize the precoding and common rate allocation to maximize the RE of RSMA-aided VLC networks, while satisfying the QoS constraints and the LED linear operation range constraints. To solve this fractional problem, we first adopt the quadratic transformation technique to convert the fractional objective function to a concave one. Subsequently, fractional programming (FP) is adopted to transform the non-convex problem into a tractable one. Finally, by introducing auxiliary variables and penalty function, the problem is addressed by the primal-dual-gradient-based algorithm.
- To overcome the practical challenges posed by imperfect CSI in VLC systems, we propose an SCA-based robust algorithm for the worst-case transmission design while ensuring the QoS performance of the systems. To address the issue of robust optimization, SDR technique combined with $\mathcal{S}$-lemma are adopted to transform non-convex constraints into a series of linear matrix inequalities (LMI). Finally, the worst-case robust precoding design and common rate allocation problem is effectively settled by the introduced SCA-based algorithm.
- The simulation results demonstrate that the proposed precoding strategy for RSMA-based VLC systems surpasses the existing baseline schemes. More specifically, the proposed RE algorithm achieves a well-balanced tradeoff between EE and SE. Furthermore, the RSMA-based scheme always exhibits a higher resource efficiency than NOMA and SDMA. In scenarios with imperfect CSI, the proposed worst-case RSMA scheme outperforms non-robust designs in terms of resource efficiency.

The remainder of this work is structured as follows. Section II provides a characterization of the RSMA-aided VLC system model and introduces the RE metric. In Section III, we explore the joint precoding design and common rate allocation for optimizing RE in perfect CSI scenarios while Section IV investigates the worst-case robust precoding strategy under imperfect CSI. Simulation results are presented in Section V, followed by a conclusion in Section VI.

II. System Model

A. Signal Model

In this paper, we investigate a downlink VLC system, which applies RSMA to eliminate multi-user interference. The system comprises of one VLC base station (BS) with N LEDs and K users each equipped with a single photodetector. The concept of RSMA-VLC is depicted in Fig. 1. Specifically, the intended message U_k for kth user is divided into two components, namely a common component $U_{c,k}$ and a private component $U_{p,k}$. All users' common components are superimposed and encoded together into a shared common stream s_0. The private components $U_{p,k}$ are separately encoded into the private streams s_k for each user. Asssuming that s_k is normalized to the range [-1, 1] with zero mean and σ_s^2 variance.

At the VLC BS, the transmitted signal is given by

This article has been accepted for publication in IEEE Photonics Journal. This is the author's version which has not been fully edited and content may change prior to final publication. Citation information: DOI 10.1109/JPHOT.2024.3388472

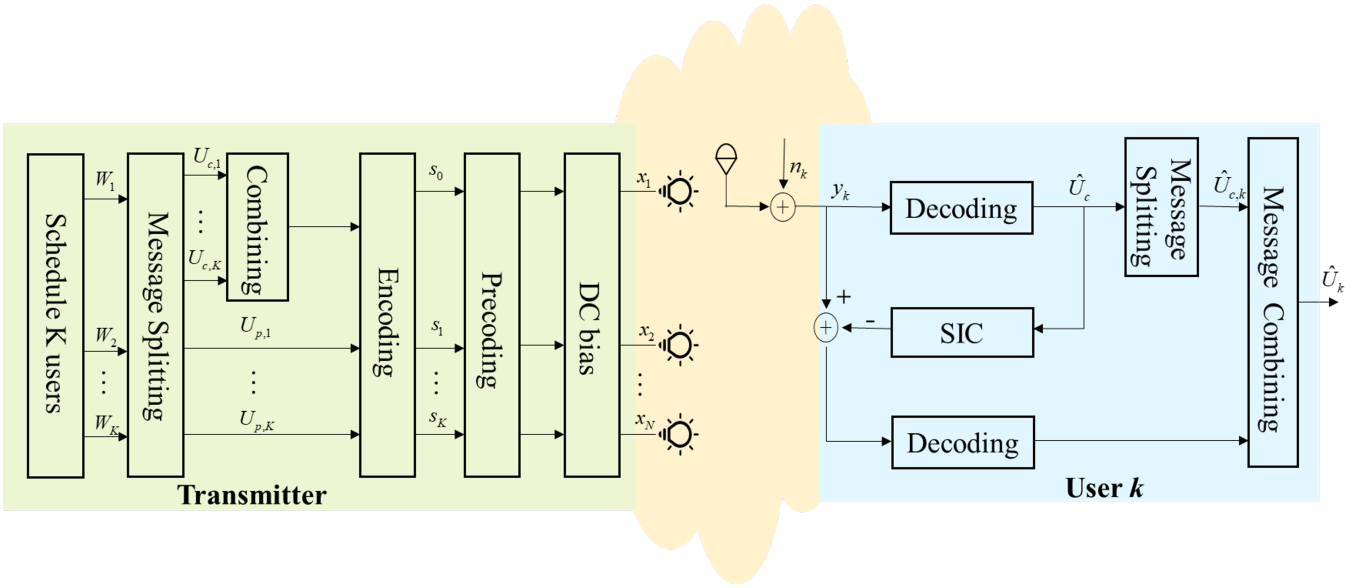

Fig. 1: Diagram of RSMA-based VLC systems.

$$\mathbf{x} = \mathbf{w}_0 s_0 + \sum_{j=1}^{K} \mathbf{w}_j s_j + \mathbf{I}_{dc} \tag{1}$$

where $\mathbf{w}_0$ denotes the precoding vector of common signal s_0 and $\mathbf{w}_k$ denotes the precoding vector of private signal s_k. $\mathbf{I}_{dc} = [I_{dc}, \cdots, I_{dc}]^T$ is the direct current (DC) bias to ensure a positive electrical signal, which is essential for LEDs. To meet the dynamic operation range and the illumination requirements of LED, the constraints on precoding matrix $\mathbf{W} = [\mathbf{w}_0, \mathbf{w}_1, \cdots, \mathbf{w}_K]$ are expressed by

$$\|\mathbf{W}(n,:)\|_1 \leq \min\{I_{dc} - I_{min}, I_{max} - I_{dc}\} \triangleq I, \forall n \tag{2}$$

where I_{min} and I_{max} are the minimum and maximum allowable current in the LED linear operation range, respectively.

The DC bias, which does not carry any information, can be removed through alternating current (AC) coupling. Once the DC-offset has been eliminated, the kth user's received signal can be represented as follows:

$$y_k = \mathbf{h}_k^T \sum_{j=0}^{K} \mathbf{w}_j s_j + n_k \tag{3}$$

where $\mathbf{h}_k$ denotes the channel matrix between the VLC BS and the kth receiver. n_k denotes the received noise which follows Gaussian distribution with the variance of σ_k^2.

The shared common signal s_0 is firstly decoded by regarding all the other private signals as noise. The SINR of decoding common rate for kth user is expressed by

$$\Gamma_{k,c} = \frac{\left|\mathbf{h}_k^T \mathbf{w}_0\right|^2}{\sum_{j=1}^{K} \left|\mathbf{h}_k^T \mathbf{w}_j\right|^2 + \sigma_k^2/\sigma_s^2} = \frac{S_{k,c}}{T_{k,c}}. \tag{4}$$

Note that the closed-form expression of channel capacity for IM/DD channel remains a mystery. In this paper, we adopt a lower bound on achievable rate as presented in [22]. The achievable common rate for kth user is expressed by

$$R_{k,c} = \frac{1}{2} \log\left(1 + \frac{6}{\pi e} \Gamma_{k,c}\right). \tag{5}$$

To guarantee that the shared common signal s_0 is successfully decoded by all receivers, the common rate should choose the worst-case common rate, given by

$$R_C = \min_k \{R_{k,c}\}. \tag{6}$$

In RSMA, all the users share the common rate R_C such that

$$\sum_{k=1}^{K} C_k = R_C \tag{7}$$

where C_k denotes the part of the shared common rate assigned to the kth user. Once the common signal s_0 is successfully decoded, user k then adopts SIC to remove common signal, and decodes its desired private signal s_k by treating the remaining private signals intended for other users as noise. Then, the SINR of decoding private rate for kth user is calculated by

$$\Gamma_{k,p} = \frac{\left|\mathbf{h}_k^T \mathbf{w}_j\right|^2}{\sum\limits_{j \neq k} \left|\mathbf{h}_k^T \mathbf{w}_j\right|^2 + \sigma_k^2/\sigma_s^2} = \frac{S_{k,p}}{T_{k,p}} \tag{8}$$

and the private rate is given by

$$R_{k,p} = \frac{1}{2} \log\left(1 + \frac{6}{\pi e} \Gamma_{k,p}\right). \tag{9}$$

B. Channel and Noise Modeling

The VLC systems employ intensity modulation at the transmitter, where the information is carried by the intensity of the light. This means that the transmitted signal must be real and non-negative. At the receivers, the optical signal is detected and converted into a proportional electrical signal through photodiode.

For the indoor scenarios, research [23] indicates that the line-of-sight (LOS) link contributes over 95% to the received power. Consequently, it is practical to concentrate on the LOS link when designing indoor VLC systems. Based on Lambert emission model, the equivalent channel coefficient between the kth receiver and the nth LED array is calculated by [19], [23], [24]

$$h_{kn} = \frac{(m+1)\,\eta_d \eta_l A_r}{2\pi d_{kn}^2} \cos^m(\phi_{kn}) \cos(\varphi_{kn})\, \Gamma(\varphi_{kn}) \quad (10)$$

where $m = -\ln 2 / \ln \cos\left(\Phi_{\frac{1}{2}}\right)$ denotes the Lambert order with $\Phi_{\frac{1}{2}}$ being the LED semi-angle. η_d and η_l denote the the detector responsivity and the LED conversion factor. A_r stands for the receiving area of the photodetector, d_{kn} is the distance between the nth LED array and the kth receiver's photodetector, ϕ_{kn} and φ_{kn} are respectively the emission angle and the incidence angle. $\Gamma(\varphi_{kn})$ denotes the optical concentrator gain obtained by

$$\Gamma(\varphi_{kn}) = \begin{cases} \frac{n^2}{\sin^2(\Psi)}, & \varphi_{kn} \le \Psi \\ 0, & \varphi_{kn} > \Psi \end{cases} \quad (11)$$

where n denotes the refractive coefficient and Ψ represents the field-of-view (FoV) of the photodetector.

The acquisition of accurate CSI is indeed challenging because of the errors in channel estimation. To characterize the estimation inaccuracy, this paper employs a norm-bounded error CSI model [25]. In particular, the actual channel for kth user is modeled as follows

$$\mathbf{h}_k = \hat{\mathbf{h}}_k + \triangle \mathbf{h}_k \quad (12)$$

where $\hat{\mathbf{h}}_k$ and $\triangle \mathbf{h}_k$ represent the estimated CSI vector and the bounded CSI estimation error vector, respectively. According to [26] and [27], the CSI uncertainty set can be characterized by an ellipsoid, given by

$$\mathfrak{h}_k \triangleq \left\{ \triangle \mathbf{h}_k \mid \triangle \mathbf{h}_k^T \mathbf{E}_k \triangle \mathbf{h}_k \le \epsilon_k^2 \right\} \quad (13)$$

where $\mathbf{E}_k \succeq 0$ controls the orientation of the ellipsoidal region and specifies the quality of CSI. The parameter ϵ_k^2 presenting the uncertainty controls the size of $\mathfrak{h}_k$.

For the kth receiver, the Gaussian noise n_k mainly comes from thermal disturbances, shot noise and relative-intensity fluctuations. Given the parameters mentioned above, σ_k^2 can be calculated as [19], [23], [24]

$$\sigma_k^2 = 2eB\left(P_{o,k} + 2\pi A_r \chi_{amp}\left(1 - \cos(\Psi)\right)\right) + i_{amp}^2 B \quad (14)$$

where e denotes the electron's charge, $P_{o,k} = \sum_{n=1}^{N} h_{kn} I_{dc}$ represents the average received optical power at the kth receiver, and B represents the system bandwidth. χ_{amp} and i_{amp} denote the photocurrent of ambient light and the density of noise current caused by the pre-amplifier, respectively.

C. The Definition of Resource Efficiency

The traditional system design typically focuses on SE to increase the transmission rate at all costs. The system SE refers to the amount of total throughout achieved over a limited bandwidth, with the unit of $\mathrm{bits/s/Hz}$. The definition of SE is given by

$$\mathrm{SE} = \sum_{k=1}^{K} \left(C_k + R_{k,p}\right). \quad (15)$$

The exponential growth of mobile data traffic leads to a rapid surge in the release of greenhouse gases and energy consumption. In the meanwhile, the shrinking size of terminals imposes strict limitations on battery capacity. Hence, the EE optimization has received significant research interest in practical VLC network designs, which refers to the ratio of SE to system power consumption. The system EE with the unit of $\mathrm{bits/Joule/Hz}$, is expressed by

$$\mathrm{EE} = \frac{\mathrm{SE}}{P_{\mathrm{tot}}} \quad (16)$$

where P_{tot} is the total system power consumption at the VLC BS, which is approximated as $P_{\mathrm{tot}} = \zeta \sum_{k=0}^{K} \|\mathbf{w}_k\|_2^2 + P_{VLC}$. Moreover, $\zeta \ge 1$ denotes the coefficient of power amplifier, P_{VLC} is a constant representing the power consumption of LEDs circuit and DC bias.

Both SE and EE metrics play an important role in communication system design. In certain scenarios, both SE and EE metrics should be jointly considered in communication system design. Nevertheless, EE is maximized by utilizing a portion of transmit power budget while SE uses the full transmit power budget in the moderate and high SNR regimes, which leads to a conflict. Therefore, striking a balance between them is worth considering and remains an open problem in RSMA-aided VLC systems. To this end, we consider a joint SE and EE optimization to achieve a tradeoff by maximizing a weighted sum of these two metrics. In particular, an RE metric is adopted in this paper, which is defined as [20], [28]

$$\begin{aligned} \mathrm{RE} =& \mathrm{EE} + \beta \frac{\mathrm{SE}}{P_{\mathrm{sum}}} \\ =& \left(\frac{1}{P_{\mathrm{tot}}} + \frac{\beta}{P_{\mathrm{sum}}}\right) \sum_{k=1}^{K} \left(C_k + R_{k,p}\right) \end{aligned} \quad (17)$$

where β is a weight coefficient characterizing the priority assigned to EE and SE. $\frac{1}{P_{\mathrm{sum}}}$ is the normalization factor, and P_{sum} is a constant denoting the total VLC power budget modeled as

$$P_{\mathrm{sum}} = \zeta P_{max} + P_{VLC} \quad (18)$$

where P_{max} is VLC BS transmitting power budget and ζ denotes the coefficient of power amplifier. It can be verified that the simple RE maximization equals to solve multi-objective optimization (MOO) of the EE-SE problem [20]. We can obtain various EE-SE tradeoff through adjusting the value of β. Specifically, the system designer can select a weighting factor β approaching 0 to prioritize EE while close to infinity for β when SE is given priority. Note that RE metric contains EE and SE as extreme metrics. Consequently,

investigating the EE-SE tradeoff problem for RSMA-assisted VLC systems simultaneously addresses the EE maximization and SE maximization problems.

In contrast to the previous papers solely focusing on either SE or EE, here we aim to strike a tunable balance between them. In the next sections, we explore the joint precoding design and common rate allocation for RSMA-based VLC downlink transmission to maximize the system RE in both perfect and imperfect CSI scenarios.

III. RE Maximization with Perfect CSI

The perfect CSI scenario is considered in this section, where the precoding design and common rate allocation for maximizing RE is studied. Mathematically, the RE maximization problem for RSMA-aided VLC systems can be formulated as

$$\mathrm{P1}: \max_{\mathbf{W},\mathbf{C}} \left(\frac{1}{P_{\mathrm{tot}}}+\frac{\beta}{P_{\mathrm{sum}}}\right)\sum_{k=1}^{K}\left(C_k+R_{k,p}\right) \tag{19a}$$

$$\text{s.t.} \sum_{k=1}^{K} C_k \le R_{k,c},\ C_k \ge 0, \forall k \tag{19b}$$

$$C_k + R_{k,p} \ge R_k^{\min}, \forall k \tag{19c}$$

$$\left\|\mathbf{W}\left(n,:\right)\right\|_1 \le \min\left\{I_{dc}-I_{min}, I_{max}-I_{dc}\right\}, \forall n \tag{19d}$$

where condition (19b) ensures all receivers can successfully decode the shared common stream and guarantees a non-negative achievable common rate. Eq. (19c) indicates that all users must meet the QoS requirements. Constraint (19d) ensures the LEDs work in the linear region.

The formulated problem P1 poses a challenge due to its non-convex fractional nature. In this following, we propose a primal-dual-gradient-based joint precoding and common rate allocation algorithm to tackle this non-convex problem effectively. To achieve this, we reconstruct the primal problem by means of quadratic transform and Lagrangian dual transform methods.

To deal with the complex form of $R_{k,p}$ and $R_{k,c}$ in the definition of RE, an auxiliary variable t_k is introduced to denote the total rate of kth user. The original problem P1 is thus transformed into an equivalent form as

$$\mathrm{P2}: \max_{\mathbf{W},\mathbf{C},\mathbf{t}} \left(\frac{1}{P_{\mathrm{tot}}}+\frac{\beta}{P_{\mathrm{sum}}}\right)\sum_{k=1}^{K} t_k \tag{20a}$$

$$\text{s.t.}\ C_k + R_{k,p} \ge t_k, \forall k \tag{20b}$$

$$(19b)-(19d). \tag{20c}$$

Note that problem P2 is in a form of ratio fractional sum, which can be effectively addressed by means of the quadratic transform algorithm. According to Theorem 1 in [29], it is possible to equivalently convert problem P2 into

$$\mathrm{P3}: \max_{\mathbf{W},\mathbf{C},\mathbf{t},\mathbf{y}} \sum_{k=1}^{K}\left(2y_k\sqrt{t_k}-y_k^2 P_{tot}\right)+\frac{\beta}{P_{sum}}\sum_{k=1}^{K} t_k \tag{21a}$$

$$\text{s.t.}\ (20b), (20c) \tag{21b}$$

where $\{y_k\}$ is the set of slack variables. Since P3 poses challenges in simultaneously determining the optimal values for all variables, the alternating optimization method is employed to optimize P3. More specifically, the primal variables $\{\mathbf{W},\mathbf{C}\}$ and the auxiliary variables $\{\mathbf{y},\mathbf{t}\}$ are iteratively optimized. The optimal value of $y^\star$ and $t^\star$ with fixed $\{\mathbf{W},\mathbf{C}\}$ can be obtained in the closed-form as

$$y_k^\star = \frac{\sqrt{t_k}}{P_{\mathrm{tot}}\left(\mathbf{W}\right)} \tag{22a}$$

$$t_k^\star = C_k + R_{k,p}\left(\mathbf{W}\right) \tag{22b}$$

Then, we optimize $\{\mathbf{W},\mathbf{C}\}$ with given $\{\mathbf{y},\mathbf{t}\}$. The Lagrangian dual transform and quadratic transform [29] is adopted to reformulate the common rate and private rate as

$$f_{k,c}\left(\mathbf{W},\gamma_{k,c},\alpha_{k,c}\right) = \left(1+\gamma_{k,c}\right)-\gamma_{k,c}+2\alpha_{k,c}\sqrt{1+\gamma_{k,c}} \times\left(\sqrt{\frac{6}{\pi e}}\mathbf{h}_k^T\mathbf{w}_0\right)-\alpha_{k,c}^2\left(\frac{6}{\pi e}S_{k,c}+T_{k,c}\right) \tag{23a}$$

$$f_{k,p}\left(\mathbf{W},\gamma_{k,p},\alpha_{k,p}\right) = \left(1+\gamma_{k,p}\right)-\gamma_{k,p}+2\alpha_{k,p}\sqrt{1+\gamma_{k,p}} \times\left(\sqrt{\frac{6}{\pi e}}\mathbf{h}_k^T\mathbf{w}_j\right)-\alpha_{k,p}^2\left(\frac{6}{\pi e}S_{k,p}+T_{k,p}\right) \tag{23b}$$

where $\{S_{k,c},T_{k,c},S_{k,p},T_{k,p}\}$ is defined in (4) and (8). With given $\{\mathbf{y},\mathbf{t}\}$, the problem P3 is equivalent to

$$\mathrm{P4}: \min_{\Phi} \zeta\sum_{k=0}^{K}\left\|\mathbf{w}_k\right\|_2^2+P_{VLC} \tag{24a}$$

$$\text{s.t.} \sum_{k=1}^{K} C_k \le \frac{f_{k,c}\left(\mathbf{W},\gamma_{k,p},\alpha_{k,c}\right)}{2},\ C_k \ge 0, \forall k \tag{24b}$$

$$C_k+\frac{1}{2}f_{k,p}\left(\mathbf{W},\gamma_{k,p},\alpha_{k,c}\right) \ge R_k^{\min}, \forall k \tag{24c}$$

$$(19d) \tag{24d}$$

where $\Phi=\{\mathbf{W},\mathbf{C},\boldsymbol{\gamma},\boldsymbol{\alpha}\}$ is the optimization variables set. Problem P4 demonstrates block coordinate-wise convexity. Therefore, we propose an alternating optimization method to solve problem P4. More specifically, the optimal auxiliary variables with given $\{\mathbf{W},R_C\}$ can be obtained by

$$\gamma_{k,c}^\star = \frac{6}{\pi e}\frac{\left|\mathbf{h}_k^T\mathbf{w}_0\right|^2}{T_{k,c}} \tag{25a}$$

$$\gamma_{k,p}^\star = \frac{6}{\pi e}\frac{\left|\mathbf{h}_k^T\mathbf{w}_k\right|^2}{T_{k,p}} \tag{25b}$$

$$\alpha_{k,c}^\star = \frac{\sqrt{\left(1+\gamma_{k,c}\right)}\left(\sqrt{\frac{6}{\pi e}}\mathbf{h}_k^T\mathbf{w}_0\right)}{\frac{6}{\pi e}\left|\mathbf{h}_k^T\mathbf{w}_0\right|^2+T_{k,c}} \tag{25c}$$

$$\alpha_{k,p}^\star = \frac{\sqrt{\left(1+\gamma_{k,p}\right)}\left(\sqrt{\frac{6}{\pi e}}\mathbf{h}_k^T\mathbf{w}_j\right)}{\frac{6}{\pi e}\left|\mathbf{h}_k^T\mathbf{w}_k\right|^2+T_{k,p}}. \tag{25d}$$

For fixed $\{\boldsymbol{\gamma},\boldsymbol{\alpha}\}$, the optimal $\{\mathbf{W},R_C\}$ can be obtained by addressing the following problem:

$$L(\Phi)=\sum_{k=0}^{K}\|\mathbf{w}_k\|_2^2+\frac{\rho}{2}\sum_{k=1}^{K}|T_k-C_k|^2+\sum_{k=1}^{K}\alpha_k\left(T_k-C_k\right)+\sum_{k=1}^{K}\lambda_k\left(\sum_{k=1}^{K}T_k-\frac{1}{2}f_{k,c}\left(\mathbf{W}\right)\right)+\sum_{n=1}^{N}\mu_n\left(\sum_{k=0}^{K}\mathrm{Tr}\left(\mathbf{w}_k\mathbf{w}_k^T\mathbf{E}_n\right)-\frac{I^2}{K+1}\right)+\sum_{k=1}^{K}v_k\left(R_k^{\min}-C_k-\frac{1}{2}f_{k,p}\left(\mathbf{W}\right)\right) \tag{28}$$

$$\mathbf{w}_0^{m+1}=\left(\sum_j\lambda_j^m\left(\alpha_{k,c}^m\right)^2\frac{6}{\pi e}\mathbf{h}_j\mathbf{h}_j^T+\sum_{n=1}^{N}2\mu_n^m\mathbf{E}_n+2\mathbf{I}\right)^{+}\sum_j\lambda_j^m\alpha_{j,c}^m\sqrt{1+\gamma_{j,c}}\sqrt{\frac{6}{\pi e}}\mathbf{h}_j \tag{29}$$

$$\mathbf{w}_k^{m+1}=\left(\sum_{j=1}^{K}\frac{6}{\pi e}\lambda_j^m\left(\alpha_{j,c}^m\right)^2\mathbf{h}_j\mathbf{h}_j^T+\sum_{n=1}^{N}2\mu_n^m\mathbf{E}_n+\sum_{j\neq k}\nu_j^m\left(\alpha_{j,p}^m\right)^2\mathbf{h}_j\mathbf{h}_j^T+\frac{6}{\pi e}\left(\alpha_{k,p}^m\right)^2\nu_k^m\mathbf{h}_k\mathbf{h}_k^T+2\mathbf{I}\right)^{+} \times\alpha_{k,p}^m\nu_k^m\sqrt{1+\gamma_{k,p}}\sqrt{\frac{6}{\pi e}}\mathbf{h}_k \tag{30}$$

$$\mathrm{P5}:\min_{\mathbf{W},\mathbf{C}}\ \zeta\sum_{k=0}^{K}\|\mathbf{w}_k\|_2^2+P_{VLC} \tag{26a}$$

$$\text{s.t.}\ \sum_{k=1}^{K}C_k\le\frac{1}{2}f_{k,c}\left(\mathbf{W}\right),\ C_k\ge0,\forall k \tag{26b}$$

$$C_k+\frac{1}{2}f_{k,p}\left(\mathbf{W}\right)\ge R_k^{\min},\forall k \tag{26c}$$

$$(19d) \tag{26d}$$

As can be observed from P5, the reformulated problem P5 exhibits convexity which can be effectively solved by the CVX package. However, the utilization of CVX results in a significant increase in computational complexity. The primal-dual gradient method [30] is a straightforward yet potent technique that effectively tackles large-scale optimization problems by decomposing them into smaller subproblems, thereby facilitating their handling. First, we relax problem P5 by introducing auxiliary variables $\{T_k\}$ and transform it into the following problem:

$$\mathrm{P6}:\min_{\mathbf{W},\mathbf{C},\mathbf{T}}\ \sum_{k=0}^{K}\|\mathbf{w}_k\|_2^2 \tag{27a}$$

$$\text{s.t.}\ T_k=C_k,\forall k \tag{27b}$$

$$\sum_{k=0}^{K}\mathrm{Tr}\left(\mathbf{w}_k\mathbf{w}_k^T\mathbf{E}_n\right)\le\frac{I^2}{K+1},\forall n \tag{27c}$$

$$(26b),(26c) \tag{27d}$$

The augmented Lagrangian function of P6 can be given by (28) at the top of this page, where $\rho>0$ is the penalty parameter.

By setting the derivative of the augmented Lagrangian function to 0, the precoding matrix, common rate allocation vector and dual variables can be updated by (29)-(31f):

$$T_k^{m+1}=C_k^m-\frac{1}{\rho}\left(\sum_{k=1}^{K}\lambda_k^m+\alpha_k^m\right) \tag{31a}$$

$$C_k^{m+1}=T_k^{m+1}+\frac{1}{\rho}\left(v_k^m+\alpha_k^m\right) \tag{31b}$$

$$\alpha_k^{m+1}=\alpha_k^m+\rho\left(T_k^{m+1}-C_k^{m+1}\right) \tag{31c}$$

$$\lambda_k^{m+1}=\lambda_k^m+\rho\left(\sum_{k=1}^{K}T_k^{m+1}-\frac{1}{2}f_{k,c}\left(\mathbf{W}^{m+1}\right)\right) \tag{31d}$$

$$\nu_k^{m+1}=\nu_k^m+\rho\left(R_k^{\min}-C_k^{m+1}-\frac{1}{2}f_{k,p}\left(\mathbf{W}^{m+1}\right)\right) \tag{31e}$$

$$\mu_n^{m+1}=\mu_n^{m+1}+\rho\left(\sum_{k=0}^{K}\mathrm{Tr}\left(\mathbf{w}_k^{m+1}\left(\mathbf{w}_k^{m+1}\right)^T\mathbf{E}_n\right)-\frac{I^2}{K+1}\right). \tag{31f}$$

Algorithm 1 Precoding Design and Common Rate Allocation for RE Maximization.

1: Initialization: error tolerance ϵ_1 and iteration index $m=0$.
2: **repeat**
3: For fixed $\{\mathbf{W},\mathbf{C}\}$, update y_k and t_k by (22a) and (22b).
4: **repeat**
5: For fixed $\{\boldsymbol{\gamma},\boldsymbol{\alpha}\}$, solve P5 by (29)-(31f).
6: Update $\{\boldsymbol{\gamma},\boldsymbol{\alpha}\}$ by (25a)-(25d) and set $l=l+1$.
7: **until** Convergence.
8: Calculate $\mathrm{RE}_m=\left(\frac{1}{P_{\mathrm{tot}}}+\frac{\beta}{P_{\mathrm{sum}}}\right)\sum_{k=1}^{K}\left(C_k+R_{k,p}\right)$.
9: Update $\mathbf{\Psi}^{m+1}$=$\mathbf{\Psi}^{\mathrm{temp}}$ and set $m=m+1$.
10: **until** $|\mathrm{RE}_m-\mathrm{RE}_{m-1}|\le\epsilon_1$.
11: Return the beamforming matrix $\mathbf{W}$ and common rate allocation vector $\mathbf{C}$.

Complexity Analysis: In Algorithm 1, the results are obtained by an alternating optimization. In the proposed Algorithm 1, the main computational complexity arises from the primal-dual-gradient algorithm for updating the precoding

vector and dual variables. The complexity of updating the precoding vector is $O\left(K\left(KN^2+N^3+N^2\right)\right)$ and the complexity of updating the dual variables is $O\left(KN^2\right)$. Assume Algorithm 1 converges after N_i iterations and the primal-dual-gradient algorithm converges after N_o iterations. The computational complexity of is $O\left(N_iN_o\left(KN^3+K^2N^2\right)\right)$.

IV. Extension to Imperfect CSI Scenarios

The preceding section focused on investigating the joint precoding design and common rate allocation of the RSMA-based VLC system with ideal CSI. However, the CSI estimation errors is always inevitable for practical VLC networks due to feedback delay, channel estimation errors and quantization errors, which will result in residual interference during SIC operations and severely affect the VLC network's performance. Taking this into consideration, we further explore the joint precoding design and common rate allocation of the RSMA-based VLC systems in the context of imperfect CSI.

The worst-case common rate and private rate for user k are given by (37) and (38), respectively, as demonstrated at the top of next page. It is crucial to note that the common signal s_0 is removed by SIC. In the presence of imperfect CSI, the users can not completely remove the common signal, which leads to the residual term $\triangle\mathbf{h}_k^T\mathbf{w}_0$ in (38).

The previous work is now extended to more practical scenarios where errors occur in channel estimation. Building upon the closed-form expressions of worst-case rate (37) and (38), we concentrate on joint robust precoding design and common message rate allocation to maximize resource efficiency while taking into account the QoS constraints, LoR constraints and imperfect CSI. Mathematically, the optimization problem for maximizing worst-case resource efficiency under imperfect CSI is formulated as follows:

$$\mathrm{P7}: \max_{\mathbf{W},\mathbf{C}} \left(\frac{1}{P_{\mathrm{tot}}}+\frac{\beta}{P_{\mathrm{sum}}}\right)\sum_{k=1}^{K}\left(C_k+R_{k,p}^{\mathrm{worst}}\right) \tag{32a}$$

$$\text{s.t.} \sum_{k=1}^{K} C_k \le R_{k,c}^{\mathrm{worst}},\ C_k \ge 0, \forall k \tag{32b}$$

$$C_k + R_{k,p}^{\mathrm{worst}} \ge R_k^{\min}, \forall k \tag{32c}$$

$$\left\|\mathbf{W}\left(n,:\right)\right\|_1 \le \min\left\{I_{dc}-I_{min}, I_{max}-I_{dc}\right\}, \forall n \tag{32d}$$

$$\triangle\mathbf{h}_k^T\mathbf{E}_k\triangle\mathbf{h}_k \le \epsilon_k^2, \forall k \tag{32e}$$

In the beamforming design and common rate allocation problem, constraint (32b) ensures that all receivers are able to decode the shared common stream s_0 correctly. Constraint (32c) guarantees all receivers can meet the minimum QoS demands. Constraint (32d) ensures that the LEDs work in the linear operation region. The challenges in solving the non-convex fractional problem P5 primarily lie in two aspects: 1) the channel uncertainty constraint (32e) involves in fact infinitely many constraints; 2) the complicated form of $R_{k,c}$ and $R_{k,p}$ makes the problem non-convex.

Like the perfect CSI scenario, we first adopt auxiliary variables, quadratic transform and SDR to deal with the complicated form of objective function and constraints. The reformulated problem is expressed by

$$\mathrm{P8}: \max_{\mathbf{W},\mathbf{C},\mathbf{t}} \sum_{k=1}^{K}\left(2y_k\sqrt{t_k}-y_k^2P_{\mathrm{tot}}\right)+\frac{\beta}{P_{\mathrm{sum}}}\sum_{k=1}^{K}t_k \tag{33a}$$

$$\text{s.t. } C_k + R_{k,p}^{\mathrm{worst}} \ge t_k, \forall k \tag{33b}$$

$$\sum_{k=1}^{K} C_k \le R_{k,c}^{\mathrm{worst}},\ C_k \ge 0, \forall k \tag{33c}$$

$$C_k + R_{k,p}^{\mathrm{worst}} \ge R_k^{\min}, \forall k \tag{33d}$$

$$\sum_{k=0}^{K}\mathrm{Tr}\left(\mathbf{Q}_k\mathbf{E}_n\right) \le \frac{I^2}{K+1}, \forall n \tag{33e}$$

$$\triangle\mathbf{h}_k^T\mathbf{E}_k\triangle\mathbf{h}_k \le \epsilon_k^2, \forall k \tag{33f}$$

The constraints (33b), (33c) and (33d) contribute to the non-convexity of P6. To deal with this problem, we introduce equivalence transformation to replace the worst-case common and private rate of user k.

$$(33b) \Leftrightarrow C_k + R_{k,p} \ge t_k,\ \forall k,\ \forall\triangle\mathbf{h}_k \tag{34a}$$

$$(33c) \Leftrightarrow \sum_{k=1}^{K} C_k \le R_{k,c},\ \forall k,\ \forall\triangle\mathbf{h}_k \tag{34b}$$

$$(33d) \Leftrightarrow C_k + R_{k,p} \ge R_k^{\min},\ \forall k,\ \forall\triangle\mathbf{h}_k \tag{34c}$$

We then introduce exponential variables for the the achievable private rate $R_{k,p}$ and common rate $R_{k,c}$ [16]. The auxiliary exponential variables $\{\mathbf{a}_{k,p},\mathbf{a}_{k,c},\mathbf{b}_{k,p},\mathbf{b}_{k,c}\}$ are introduced to enable approximating (34a), (34b), (34c) as a convex constraint.

$$e^{b_{k,c}} \ge T_{k,c}, \forall\triangle\mathbf{h}_k \tag{35a}$$

$$e^{b_{k,p}} \ge T_{k,p}, \forall\triangle\mathbf{h}_k \tag{35b}$$

$$e^{a_{k,c}} \le \frac{6}{\pi e}\left|\mathbf{h}_k^T\mathbf{w}_0\right|^2 + T_{k,c}, \forall\triangle\mathbf{h}_k \tag{35c}$$

$$e^{a_{k,p}} \le \frac{6}{\pi e}\left|\mathbf{h}_k^T\mathbf{w}_k\right|^2 + T_{k,p}, \forall\triangle\mathbf{h}_k \tag{35d}$$

By employing the slack exponential variables for (33b)-(33d), P6 can be reformulated as follows

$$\mathrm{P8}: \max_{\Omega} \sum_{k=1}^{K}\left(2y_k\sqrt{t_k}-y_k^2P_{\mathrm{tot}}\right)+\frac{\beta}{P_{\mathrm{sum}}}\sum_{k=1}^{K}t_k \tag{36a}$$

$$\text{s.t.} \sum_{k=1}^{K} C_k \le \frac{1}{2\ln 2}\left(a_{k,c}-b_{k,c}\right),\ C_k \ge 0, \forall k \tag{36b}$$

$$C_k + \frac{1}{2\ln 2}\left(a_{k,p}-b_{k,p}\right) \ge t_k, \forall k \tag{36c}$$

$$C_k + \frac{1}{2\ln 2}\left(a_{k,p}-b_{k,p}\right) \ge R_k^{\min}, \forall k \tag{36d}$$

$$(33e), (35a), (35b), (35d), (35d) \tag{36e}$$

where $\mathbf{\Omega}=\{\mathbf{Q},\mathbf{C},\mathbf{t},\mathbf{a}_p,\mathbf{b}_p,\mathbf{a}_c,\mathbf{b}_c\}$ is the optimization variables set. The problem P8 remains non-convex and computationally intractable due to the presence of infinitely many constraints within constraints (35a)-(35d). By substituting the CSI error model (12) into (35a)-(35d) and introducing the

$$R_{k,c}^{\text{worst}} = \min_{\triangle \mathbf{h}_k \in \mathfrak{h}_k} R_{k,c} = \min_{\triangle \mathbf{h}_k \in \mathfrak{h}_k} \frac{1}{2} \log \left(1 + \frac{\frac{6}{\pi e} \left| \left(\hat{\mathbf{h}}_k^T + \triangle \mathbf{h}_k^T \right) \mathbf{w}_0 \right|^2}{\sum_{j \in \mathcal{K}} \left| \left(\hat{\mathbf{h}}_k^T + \triangle \mathbf{h}_k^T \right) \mathbf{w}_j \right|^2 + \sigma_k^2} \right) \tag{37}$$

$$R_{k,p}^{\text{worst}} = \min_{\triangle \mathbf{h}_k \in \mathfrak{h}_k} R_{k,p} = \min_{\triangle \mathbf{h}_k \in \mathfrak{h}_k} \frac{1}{2} \log \left(1 + \frac{\frac{6}{\pi e} \left| \left(\hat{\mathbf{h}}_k^T + \triangle \mathbf{h}_k^T \right) \mathbf{w}_k \right|^2}{\sum_{j \neq k} \left| \left(\hat{\mathbf{h}}_k^T + \triangle \mathbf{h}_k^T \right) \mathbf{w}_j \right|^2 + \left| \triangle \mathbf{h}_k^T \mathbf{w}_0 \right|^2 + \sigma_k^2} \right) \tag{38}$$

slack variables $\{\mathbf{u}_{k,p}, \mathbf{v}_{k,p}, \mathbf{u}_{k,c}, \mathbf{v}_{k,c}\}$, constraints (35a)-(35d) can be rewritten by as follows:

$$u_{k,c} \leq \triangle \mathbf{h}_k^T \mathbf{R} \triangle \mathbf{h}_k + 2 \triangle \mathbf{h}_k^T \mathbf{R} \hat{\mathbf{h}}_k + \mathbf{h}_k^T \mathbf{R} \hat{\mathbf{h}}_k + \sigma_k^2 \tag{39a}$$

$$v_{k,c} \geq \triangle \mathbf{h}_k^T \mathbf{B} \triangle \mathbf{h}_k + 2 \triangle \mathbf{h}_k^T \mathbf{B} \hat{\mathbf{h}}_k + \mathbf{h}_k^T \mathbf{B} \hat{\mathbf{h}}_k + \sigma_k^2 \tag{39b}$$

$$u_{k,p} \leq \triangle \mathbf{h}_k^{\mathrm{T}} \mathbf{R} \triangle \mathbf{h}_k + 2 \triangle \mathbf{h}_k^T \bar{\mathbf{R}} \hat{\mathbf{h}}_k + \hat{\mathbf{h}}_k^{\mathrm{T}} \bar{\mathbf{R}} \hat{\mathbf{h}}_k + \sigma_k^2 \tag{39c}$$

$$v_{k,p} \geq \triangle \mathbf{h}_k^T \tilde{\mathbf{B}} \triangle \mathbf{h}_k + 2 \triangle \mathbf{h}_k^T \bar{\mathbf{B}} \hat{\mathbf{h}}_k + \hat{\mathbf{h}}_k^{\mathrm{T}} \bar{\mathbf{B}} \hat{\mathbf{h}}_k + \sigma_k^2 \tag{39d}$$

$$e^{a_{k,c}} \leq u_{k,c},\ e^{b_{k,c}} \geq v_{k,c},\ e^{a_{k,p}} \leq u_{k,p},\ e^{b_{k,p}} \geq v_{k,p} \tag{39e}$$

where $\mathbf{R} = \frac{6}{\pi e} \mathbf{Q}_0 + \sum_{i=1}^{K} \mathbf{Q}_i$, $\bar{\mathbf{R}} = \frac{6}{\pi e} \mathbf{Q}_k + \sum_{i \neq k} \mathbf{Q}_i$, $\mathbf{B} = \sum_{j=1}^{K} \mathbf{Q}_j$, $\tilde{\mathbf{B}} = \frac{6}{\pi e} \mathbf{Q}_k + \frac{6}{\pi e} \mathbf{Q}_0 + \sum_{i \neq k} \mathbf{Q}_i$, $\bar{\mathbf{B}} = \sum_{j=1, j \neq k}^{K} \mathbf{Q}_j$. Next, we employ $\mathcal{S}$-Procedure [31] to convert the countless constraints into a set of linear matrix inequalities.

Based on $\mathcal{S}$-Procedure [31], we transform (39a)-(39d) into a finite number of LMI constraints by applying $\mathcal{S}$-Procedure, which can be given by

$$\begin{bmatrix} \gamma_{k,c} \mathbf{I} + \mathbf{R} & \mathbf{R} \hat{\mathbf{h}}_k \\ \hat{\mathbf{h}}_k^T \mathbf{R} & -\gamma_{k,c} v_k + \hat{\mathbf{h}}_k^T \mathbf{R} \hat{\mathbf{h}}_k + \sigma_k^2 - u_{k,c} \end{bmatrix} \succeq 0 \tag{40a}$$

$$\begin{bmatrix} \lambda_{k,c} \mathbf{I} - \mathbf{B} & -\mathbf{B} \hat{\mathbf{h}}_k \\ -\hat{\mathbf{h}}_k^T \mathbf{B} & -\lambda_{k,c} v_k - \hat{\mathbf{h}}_k^T \mathbf{B} \hat{\mathbf{h}}_k - \sigma_k^2 + v_{k,c} \end{bmatrix} \succeq 0 \tag{40b}$$

$$\begin{bmatrix} \gamma_{k,p} \mathbf{I} + \mathbf{R} & \bar{\mathbf{R}} \hat{\mathbf{h}}_k \\ -\hat{\mathbf{h}}_k^T \bar{\mathbf{R}} & -\gamma_{k,p} v_k + \hat{\mathbf{h}}_k^{\mathrm{T}} \bar{\mathbf{R}} \hat{\mathbf{h}}_k + \sigma_k^2 - u_{k,p} \end{bmatrix} \succeq 0 \tag{40c}$$

$$\begin{bmatrix} \lambda_{k,p} \mathbf{I} - \tilde{\mathbf{B}} & -\bar{\mathbf{B}} \hat{\mathbf{h}}_k \\ -\hat{\mathbf{h}}_k^T \bar{\mathbf{B}} & -\lambda_{k,p} v_k - \hat{\mathbf{h}}_k^{\mathrm{T}} \bar{\mathbf{B}} \hat{\mathbf{h}}_k - \sigma_k^2 + v_{k,p} \end{bmatrix} \succeq 0 \tag{40d}$$

where $\gamma_{k,c} \geq 0$, $\lambda_{k,c} \geq 0$, $\gamma_{k,p} \geq 0$, and $\lambda_{k,p} \geq 0$ are slack variables. Up to now, most of the constraints are convex except for (39e). To tackle these non-convex constraints, SCA is adopted to approximate the exponential bounds. For (39e), it can be linearly approximated by employing the affine Taylor expansion as

$$e^{b_{k,c}^{[m-1]}} + e^{b_{k,c}^{[m-1]}} \left(b_{k,c}^{[m]} - b_{k,c}^{[m-1]} \right) \geq v_{k,c} \tag{41a}$$

$$e^{b_{k,p}^{[m-1]}} + e^{b_{k,p}^{[m-1]}} \left(b_{k,p}^{[m]} - b_{k,p}^{[m-1]} \right) \geq v_{k,p} \tag{41b}$$

where $b_{k,c}^{[m]}$ and $b_{k,p}^{[m]}$ are feasible solutions obtained at the mth iteration. Based on the $\mathcal{S}$-lemma and SCA method, P7 with an infinite number of constraints can be finally approximated at the mth iteration as the following convex sub-problem

$$\text{P9}: \max_{\mathbf{\Omega}} \sum_{k=1}^{K} \left(2 y_k \sqrt{t_k} - y_k^2 P_{\text{sum}} \right) + \frac{\beta}{P_{\text{tot}}} \sum_{k=1}^{K} t_k \tag{42a}$$

$$\text{s.t.}\ (36b), (36c), (36d), (36e) \tag{42b}$$

$$(40a), (40b), (40c), (40d) \tag{42c}$$

$$(41a), (41b) \tag{42d}$$

With given feasible initial value, the reformulated problem P8 is then iteratively linearized as a convex problem which can be solved by using standard CVX package [32] until convergence is achieved. Once the solution set $\mathcal{Q}$ is obtained, the rank of $\mathbf{Q}_k$ should be checked. If the rank of $\mathbf{Q}_k$ is one, then the solution $\mathbf{w}_k$ to P5 can be recovered from the eigenvector of $\mathbf{Q}_k$ corresponding to the largest eigenvalue. Otherwise, a near-optimal solution can be obtained utilizing a Gaussian randomization technique. The SCA-based robust precoding and common rate allocation algorithm is outlined in Algorithm 2. With respect to Algorithm 2, the overall computational complexity is approximated by $O\left(N_i N_o \left(N^2 (K+1)^2 + 14K \right)^{3.5} \right)$.

Theorem 1: The sequence $\{\mathbf{\Omega}^m\}$ generated by Algorithm 2 exhibits convergence towards a designated limit point.

Algorithm 2 Robust Precoding Design and Common Rate Allocation for RE Maximization.

1: Initialization: index $i = 0$ and error tolerance δ_2.
2: **repeat**
3: For fixed $\mathbf{\Psi}$, update $y_k^\star = \frac{\sqrt{t_k^n}}{P_{\text{sum}}(\mathbf{W}^n)}$.
4: **repeat**
5: For fixed $\mathbf{y}$, solve P8 by using CVX and obtain the solutions $\mathbf{\Omega}^{\text{temp}}$.
6: Update $\mathbf{\Omega}^{l+1}$=$\mathbf{\Omega}^{\text{temp}}$ and set $l = l + 1$.
7: **until** Convergence
8: Calculate $\text{RE}_m = \left(\frac{1}{P_{\text{tot}}} + \frac{\beta}{P_{\text{sum}}} \right) \sum_{k=1}^{K} (\delta_k C_k + R_{k,p})$.
9: Update $\mathbf{\Omega}^{m+1}$=$\mathbf{\Omega}^{\text{temp}}$ and set $m = m + 1$.
10: **until** $|\text{RE}_m - \text{RE}_{m-1}| \leq \delta_2$.
11: **if** $\text{rank}\,(\mathbf{Q}_k) == 1$ **then**
12: Calculate $\mathbf{W}$ by eigenvalue decomposition.
13: **else**
14: Calculate $\mathbf{W}$ by Gaussian randomization approach.
15: **end if**
16: Return the beamforming matrix $\mathbf{W}$ and common rate allocation vector $\mathbf{C}$.

Table I: Simulation Parameters.

Parameters	**Values**
LED semi-angle	60^{o}
Receiver FOV	60^{o}
Refractive index	1.5
PD geometrical area	1cm^2
LED conversion factor	0.44W/A
PD responsibility	0.30A/W
Ambient light photocurrent	$10.93\text{A/m}^2\text{/Sr}$
Pre-amplifier noise current density	$5\text{pA/Hz}^{-1/2}$
System Bandwidth	10MHz

Table II: LED Positions.

LEDs	Positions	LEDs	Positions
LED 1	$[1.25, 1.25, 3]$ m	LED 2	$[3.75, 1.25, 3]$ m
LED 3	$[3.75, 3.75, 3]$ m	LED 4	$[1.25, 3.75, 3]$ m
LED 5	$[1.25, 2.50, 3]$ m	LED 6	$[3.75, 2.50, 3]$ m

Proof: Please refer to Appendix.

V. Numerical Results

This section presents the simulation studies to validate the effectiveness of the proposed precoding design and common rate allocation algorithm, as well as to explore the EE-SE tradeoff in the RSMA-assisted VLC MISO systems. In our simulations, we assume a typical setup of indoor scene with the dimension of $5\text{m} \times 5\text{m} \times 3\text{m}$. The LEDs are placed at the ceiling while all users with uniform distribution are located in the receiving plane, which is set to be 0.8m. The basic parameters of the VLC network are summarized in Table I, selected from [1], [23] while the positions of LED are shown in Table II. The coefficient of power amplifier is chosen as $\zeta = 2$ and the constant power consumption is set to $P_{VLC} = 2\text{W}$. For comparison, we also consider the performance of EE optimization (EEopt) [19] and SE optimization (SEOpt) [15] as benchmarks. The solutions of EEopt scheme can be obtained by setting weighting factor $\beta = 0$ and the solutions of SEOpt scheme can be obtained by setting weighting factor $\beta \to \infty$. In the simulations, the RSMA scheme proposed in Section III is denoted as RSMA-GRA while the RSMA scheme proposed in Section IV is denoted as RSMA-SCA.

Fig. 2 and 3 compare the RE performance between RSMA, SDMA, and NOMA under both underloaded scenario and overloaded scenario with $\frac{\beta}{P_{\text{sum}}} = 1$. In the underloaded case, the VLC BS equipped with 4 LEDs (LED 1, 2, 3, 4) serves 2 users. While the system consists of 2 LEDs (LED 5, 6) and 3 users in the overloaded scenario. It can be observed that the system RE increases with the DC offset, and the RE performance of RSMA outperforms NOMA and SDMA schemes in both cases. RSMA's ability to partially decode interference and partially treat interference as noise contributes to its superior performance.

Then, we will demonstrate that the RE metric is capable of achieving the balance between EE and SE.

Fig. 4 illustrates the influence of equivalent weighting factor $\frac{\beta}{P_{\text{sum}}}$ to corresponding system EE and SE when $N = 4$ and $K = 2$. It can be observed that as the weighting factor increases, the corresponding SE rises while EE decreases. This

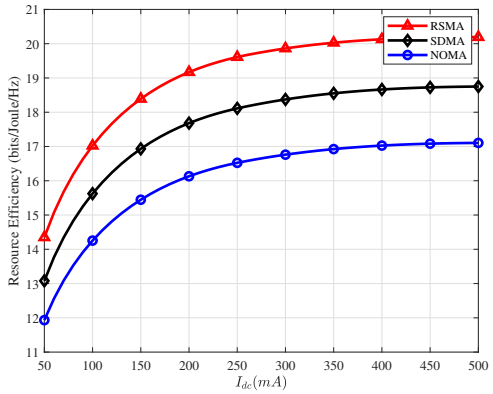

Fig. 2: The RE performance versus DC offset for underloaded scenarios with $N = 4$ and $K = 2$.

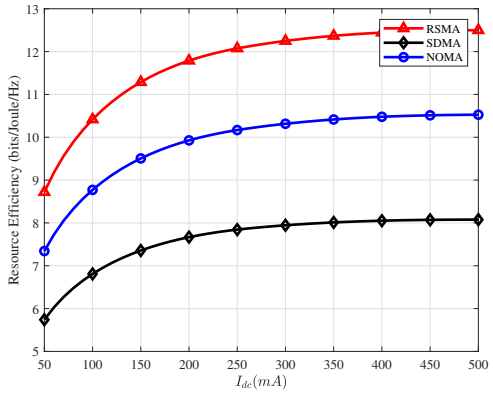

Fig. 3: The RE performance versus DC offset for overloaded scenarios with $N = 2$ and $K = 3$.

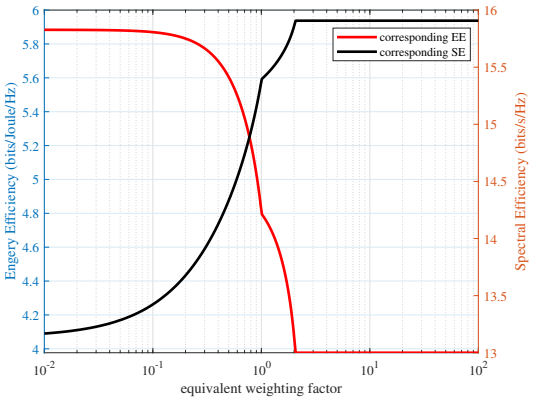

Fig. 4: Influence of the weighting factor on the corresponding system EE and SE.

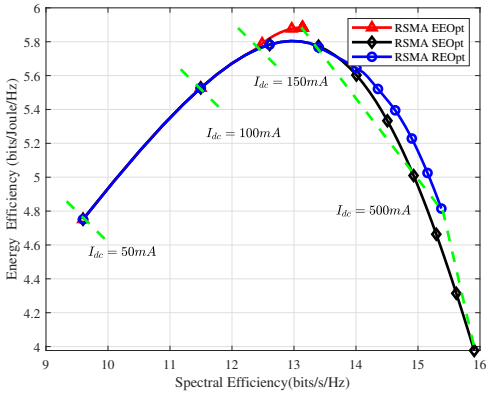

Fig. 5: EE-SE tradeoff under different DC offset.

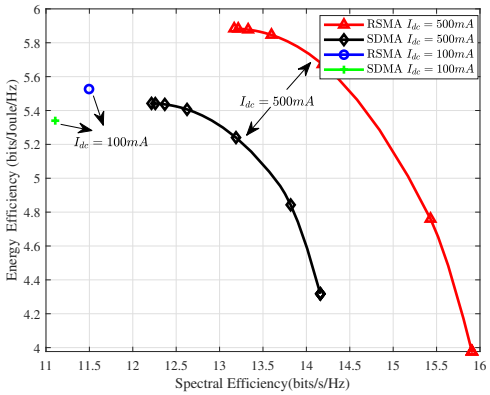

Fig. 6: EE-SE tradeoff under different weighting factor.

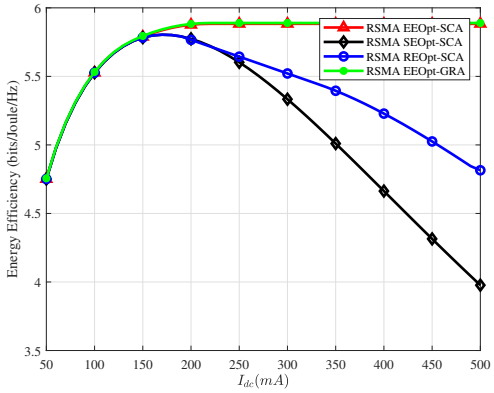

Fig. 7: Comparison between the EE performance versus DC offset.

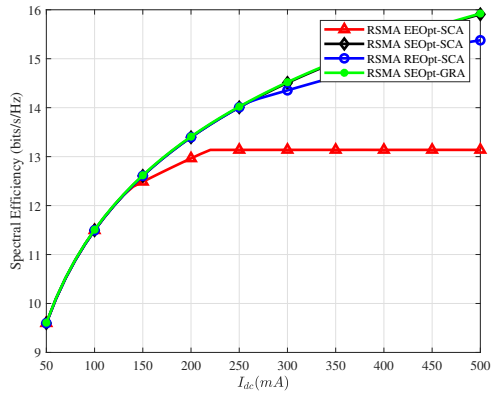

Fig. 8: Comparison between the SE performance versus DC offset.

is due to the reason that a larger weighting factor results in attaching more importance to system SE and allocate more resources to maximize the system SE. This is in accordance with the fact that when weighting factor tends to zero, the RE optimization problem degenerates to the EE optimization approach, and when weighting factor tends to infinity, it equals to the problem of maximizing SE. This means that the RE metric provides a more general framework compared with EE and SE. Fig. 4 also demonstrates the proposed RE optimization approach achieves a flexible tradeoff between EE and SE via setting an appropriate weighting factor.

Fig. 5 demonstrates the EE-SE tradeoff under different DC offset with $\frac{\beta}{P_{\text{sum}}} = 1$ when $K = 2$ and $N = 4$. For comparison, the performance of EE maximization algorithm in [19] and SE maximization algorithm in [15] are also shown. It is seen that the red curve, representing EEopt scheme, finishes when $\text{SE} = 13.18\text{bit/s/Hz}$. This is because the EEopt scheme achieves a lower SE than SEopt and REopt schemes. The result also shows that the proposed REOpt algorithm can strike a balance between the EE and SE.

Fig.6 illustrate the EE-SE tradeoff under different weighting factor. It can be seen that the SE-EE curve gathers into a point within the range of weighting factor from 10^{-2} to 10^{2} when $I_{dc} = 100\text{mA}$. That is to say, the SE and EE maintain constant when $I_{dc} = 100\text{mA}$. This is due to the fact that both EE and SE are both maximized by taking the full use of transmit power budget in the low SNR region. When $I_{dc} = 500\text{mA}$, the SE and EE achieve a tradeoff. This is due to the fact that in the moderate and high SNR regimes, SE still increases with SNR while EE starts decreasing with SNR.

To further illustrate the efficacy of the proposed REOpt algorithm, we investigate the corresponding SE and EE performance of the three approaches in relation to the DC current in Fig. 7 and 8 with $\frac{\beta}{P_{\text{sum}}} = 1$ when $K = 2$ and $N = 4$. In the low DC current budget region where $I_{dc} \leq 150\text{mA}$, we can observe that the influence of weight coefficient on EE and SE is negligible and the three considered algorithms show almost the same performance. This can be attributed to the fact that in the low DC current region, the EE and SE performance achieve the peak points with full budget, which results in the denominator of EE P_{tot} being equal to a constant and the RE and EE maximization problem degrades into the SE maximization. In contrast, the system RE maximization does not achieve either the EE or the SE maximization, but rather a tradeoff between them when I_{dc} is relatively large.

Figure 9 compares the performance of the proposed robust design and the non-robust approach under various DC offset conditions with $\frac{\beta}{P_{\text{sum}}} = 1$ when $K = 2$ and $N = 4$. The non-

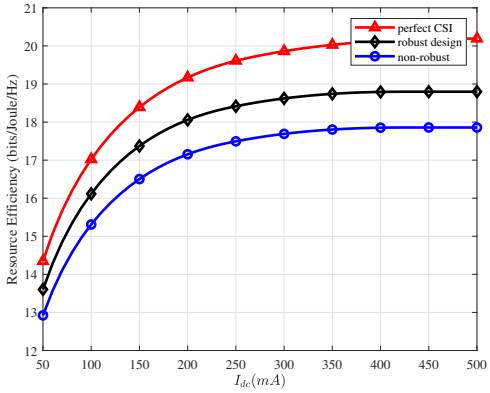

Fig. 9: The robust RE performance versus DC offset.

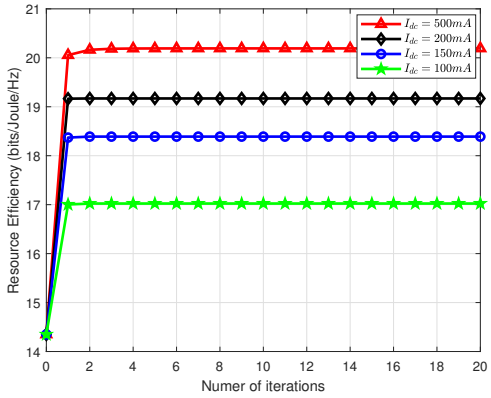

Fig. 11: Convergence of outer iteration.

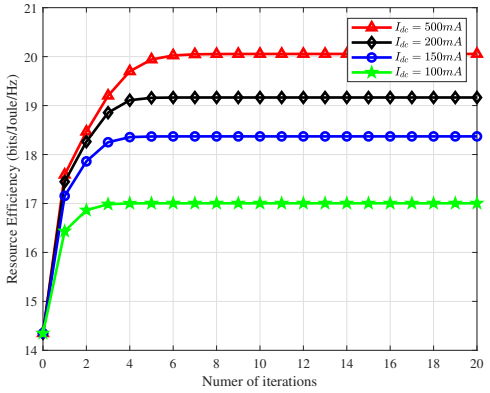

Fig. 10: Convergence of inner iteration.

Table III: Computation Time.

Setup	RSMA-GRA	RSMA-SCA
$N = 4$ and $K = 2$	2.68sec	6.53sec

robust design assumes a perfect match between the estimated and actual channels, without considering any uncertainty in the channel. Numerical results demonstrate that our developed robust algorithm achieves superior performance compared to the non-robust one by incorporating channel uncertainty for enhanced robustness.

To assess the convergence performance of the proposed RE algorithm, the resource efficiency for different DC offset in inner and outer iteration are presented in Fig. 10 and 11 with $\frac{\beta}{P_{\text{sum}}} = 1$ when $K = 2$ and $N = 4$. As illustrated in Fig. 10 and 11, the proposed SCA-based algorithm requires at most 5 inner iterations and only 1 outer iteration for convergence. In conclusion, the proposed RE algorithm exhibits rapid convergence to stationary values fast within a minimal number of iterations.

Table III compares the matlab performance time between the proposed RSMA-GRA and RSMA-SCA algorithms as a rough indicator of the computational complexity, acknowledging its limitations. It can be seen that the proposed RSMA-GRA algorithm consumes about 40% computation time of RSMA-SCA algorithm. This is due to the fact that the RSMA-GRA algorithm does not use CVX in each iteration.

VI. Conclusion

In this paper, we have investigated the RE optimization for RSMA-aided VLC MISO systems to achieve a desired EE-SE balance. We have formulated a joint precoding and common rate allocation problem to maximize the system RE, while taking into consideration of the QoS constraint and the optical power constraints of LED. To address this non-convex factional problem with perfect CSI, a primal-dual-gradient-based algorithm with low complexity has been proposed, where auxiliary variables, quadratic transform and fractional programming have been employed to transform the non-convex problem into a convex problem. Furthermore, for scenarios with imperfect CSI, we have developed a worst-case robust precoding strategy for RSMA-enhanced VLC systems to maximize the RE while ensuring the QoS requirements of all users. Specifically, by leveraging SCA and $\mathcal{S}$-Procedure techniques, a worst-case robust scheme has been proposed to yield high-quality solutions. Simulation results have demonstrated that in the low DC offset region, the system RE, SE and EE are simultaneously maximized and in the high DC offset region, the proposed RE algorithm achieves a flexible balance between EE and SE.

Appendix

The proposed RE maximization algorithm can be decomposed into two layers. For the outer optimization, the problem is solved by quadratic transform and the convergence of quadratic transform has been validated in [29]. Therefore, we focus on the proof of inner convergence. Specifically, denote the value of (21a) and (19a) as $F(\mathbf{\Psi})$ and $F^m(\mathbf{\Psi})$, respectively, where m is the iteration index. Then, we have

$$F(\mathbf{\Psi}) \geq F^m(\mathbf{\Psi}) \tag{43}$$

$$F(\mathbf{\Psi}^m) = F^m(\mathbf{\Psi}^m) \tag{44}$$

Based on (43) and (44), we have

$$\begin{aligned} F(\mathbf{\Psi}^{m+1}) \geq & F^m(\mathbf{\Psi}^{m+1}) \\ \geq & F^m(\mathbf{\Psi}^m) = F(\mathbf{\Psi}^m). \end{aligned} \tag{45}$$

The second inequality is hold due to the fact that $\mathbf{\Psi}^{m+1}$ is the optimal solution. According (45), we know that solving P4 iteratively increases the value of $F(\mathbf{\Psi})$. Moreover, $\mathbf{\Psi}^m$ is bounded by the optical power constraint (19d). Thus, it is guaranteed to convergence based on the monotone convergence theorem [14].

REFERENCES

[1] H. Ma, L. Lampe, and S. Hranilovic, "Coordinated broadcasting for multiuser indoor visible light communication systems," *IEEE Trans. Commun.*, vol. 63, no. 9, pp. 3313–3324, Jul. 2015.

[2] H. Burchardt, N. Serafimovski, D. Tsonev, S. Videv, and H. Haas, "VLC: Beyond point-to-point communication," *IEEE Commun. Mag.*, vol. 52, no. 7, pp. 98–105, Jul. 2014.

[3] H. Marshoud, S. Muhaidat, P. C. Sofotasios, S. Hussain, M. A. Imran, and B. S. Sharif, "Optical Non-Orthogonal Multiple Access for Visible Light Communication," *IEEE Wireless Commun.*, vol. 25, no. 2, pp. 82–88, Apr. 2018.

[4] X. Chen, R. Jia, and D. W. K. Ng, "On the design of massive non-orthogonal multiple access with imperfect successive interference cancellation," *IEEE Trans. Commun.*, vol. 67, no. 3, pp. 2539–2551, Nov. 2019.

[5] B. Clerckx, H. Joudeh, C. Hao, M. Dai, and B. Rassouli, "Rate splitting for MIMO wireless networks: a promising phy-layer strategy for LTE evolution," *IEEE Commun. Mag.*, vol. 54, no. 5, pp. 98–105, May 2016.

[6] Y. Mao, O. Dizdar, B. Clerckx, R. Schober, P. Popovski, and H. V. Poor, "Rate-splitting multiple access: Fundamentals, survey, and future research trends," *IEEE Commun. Surv. Tutorials*, vol. 24, no. 4, pp. 2073–2126, Jul. 2022.

[7] B. Clerckx, Y. Mao, E. A. Jorswieck, J. Yuan, D. J. Love, E. Erkip, and D. Niyato, "A Primer on Rate-Splitting Multiple Access: Tutorial, Myths, and Frequently Asked Questions," *IEEE J. Sel. Areas Commun.*, vol. 41, no. 5, pp. 1265–1308, Feb. 2023.

[8] Y. Mao, B. Clerckx, and V. O. Li, "Rate-splitting multiple access for downlink communication systems: bridging, generalizing, and outperforming SDMA and NOMA," *EURASIP J. Wireless Commun. Networking*, vol. 2018, no. 1, pp. 1–54, May 2018.

[9] J. Park, J. Choi, N. Lee, W. Shin, and H. V. Poor, "Rate-splitting multiple access for downlink MIMO: A generalized power iteration approach," *IEEE Trans. Wireless Commun.*, vol. 22, no. 3, pp. 1588–1603, Sep. 2023.

[10] T. Fang and Y. Mao, "Optimal beamforming structure for rate splitting multiple access," *arXiv preprint arXiv:2309.10342*, Dec. 2023.

[11] Y. Mao, B. Clerckx, and V. O. Li, "Energy Efficiency of Rate-Splitting Multiple Access, and performance benefits over SDMA and NOMA," in *2018 15th International Symposium on Wireless Communication Systems (ISWCS)*, Oct. 2018, pp. 1–5.

[12] Z. Yang, J. Shi, Z. Li, M. Chen, W. Xu, and M. Shikh-Bahaei, "Energy efficient Rate Splitting Multiple Access (RSMA) with Reconfigurable Intelligent Surface," in *2020 IEEE International Conference on Communications Workshops (ICC Workshops)*, Jul. 2020, pp. 1–6.

[13] G. Zhou, Y. Mao, and B. Clerckx, "Rate-Splitting Multiple Access for Multi-Antenna Downlink Communication Systems: Spectral and Energy Efficiency Tradeoff," *IEEE Trans. Wireless Commun.*, vol. 21, no. 7, pp. 4816–4828, Dec. 2022.

[14] H. Niu, Z. Lin, K. An, J. Wang, G. Zheng, N. Al-Dhahir, and K.-K. Wong, "Active RIS assisted Rate-Splitting Multiple Access Network: Spectral and Energy Efficiency Tradeoff," *IEEE J. Sel. Areas Commun.*, vol. 41, no. 5, pp. 1452–1467, Jan. 2023.

[15] S. Ma, G. Zhang, Z. Zhang, R. Gu, Y. Wu, and S. Li, "Rate Splitting Multiple Access-Aided MISO Visible Light Communications," in *2022 International Symposium on Wireless Communication Systems (ISWCS)*, 2022, pp. 1–6.

[16] S. Naser, L. Bariah, S. Muhaidat, M. Al-Qutayri, M. Uysal, and P. C. Sofotasios, "Interference Management Strategies for Multiuser Multicell MIMO VLC Systems," *IEEE Trans. Commun.*, vol. 70, no. 9, pp. 6002–6019, Jul. 2022.

[17] S. Naser, L. Bariah, W. Jaafar, S. Muhaidat, M. Al-Qutayri, M. Uysal, and P. C. Sofotasios, "Coordinated beamforming design for multi-user multi-cell MIMO VLC Networks," *IEEE Photonics J.*, vol. 14, no. 3, pp. 1–10, Apr. 2022.

[18] S. Tao, H. Yu, Q. Li, Y. Tang, and D. Zhang, "One-Layer Rate-Splitting Multiple Access with Benefits over Power-Domain NOMA in Indoor Multi-Cell Visible Light Communication Networks," in *2020 IEEE International Conference on Communications Workshops (ICC Workshops)*, 2020, pp. 1–7.

[19] F. Xing, S. He, V. C. M. Leung, and H. Yin, "Energy Efficiency Optimization for Rate-Splitting Multiple Access-Based Indoor Visible Light Communication Networks," *IEEE J. Sel. Areas Commun.*, vol. 40, no. 5, pp. 1706–1720, May 2022.

[20] J. Tang, D. K. C. So, E. Alsusa, and K. A. Hamdi, "Resource efficiency: A new paradigm on energy efficiency and spectral efficiency tradeoff," *IEEE Trans. Wireless Commun.*, vol. 13, no. 8, pp. 4656–4669, Apr. 2014.

[21] L. You, J. Xiong, A. Zappone, W. Wang, and X. Gao, "Spectral Efficiency and Energy Efficiency Tradeoff in Massive MIMO Downlink Transmission with Statistical CSIT," *IEEE Trans. Signal Process.*, vol. 68, no. 3, pp. 2645–2659, Apr. 2020.

[22] C. Sun, X. Gao, J. Wang, Z. Ding, and X.-G. Xia, "Beam Domain Massive MIMO for Optical Wireless Communications With Transmit Lens," *IEEE Trans. Commun.*, vol. 67, no. 3, pp. 2188–2202, Nov. 2019.

[23] T. Komine and M. Nakagawa, "Fundamental analysis for visible-light communication system using LED lights," *IEEE Trans. Consum. Electron.*, vol. 50, no. 1, pp. 100–107, Feb. 2004.

[24] S. Ma, H. Zhou, Y. Mao, X. Liu, Y. Wu, B. Clerckx, Y. Wang, and S. Li, "Robust beamforming design for rate splitting multiple access-aided MISO visible light communications," *arXiv preprint arXiv:2108.07014*, Nov. 2022.

[25] X. Liu, Y. Wang, F. Zhou, S. Ma, R. Q. Hu, and D. W. K. Ng, "Beamforming design for secure miso visible light communication networks with slipt," *IEEE Trans. Commun.*, vol. 68, no. 12, pp. 7795–7809, 2020.

[26] G. Zheng, K.-K. Wong, and B. Ottersten, "Robust cognitive beamforming with bounded channel uncertainties," *IEEE Trans. Signal Process.*, vol. 57, no. 12, pp. 4871–4881, Dec. 2009.

[27] G. Zheng, K.-K. Wong, and T.-S. Ng, "Robust linear mimo in the downlink: A worst-case optimization with ellipsoidal uncertainty regions," *EURASIP J. Adv. Signal Process.*, vol. 2008, pp. 1–15, Jul. 2008.

[28] W. Wang, L. Gao, R. Ding, J. Lei, L. You, C. A. Chan, and X. Gao, "Resource efficiency optimization for robust beamforming in multi-beam satellite communications," *IEEE Trans. Veh. Technol.*, vol. 70, no. 7, pp. 6958–6968, Jun. 2021.

[29] K. Shen and W. Yu, "Fractional programming for communication systems Part I: Power control and Beamforming," *IEEE Trans. Signal Process.*, vol. 66, no. 10, pp. 2616–2630, Mar. 2018.

[30] E. Esser, X. Zhang, and T. F. Chan, "A general framework for a class of first order primal-dual algorithms for convex optimization in imaging science," *SIAM J. Imag. Sci.*, vol. 3, no. 4, pp. 1015–1046, 2010.

[31] S. P. Boyd and L. Vandenberghe, *Convex optimization*. Cambridge, U.K.: Cambridge Univ. Press, 2004.

[32] M. Grant and S. Boyd, "CVX: Matlab Software for Disciplined Convex Programming, version 2.1," http://cvxr.com/cvx, Mar. 2014.